Fifth International Symposium on Marine Propulsion
SMP'17, Espoo, Finland, June 2017

Validation of a steady BEM-FEM coupled simulation with experiments on flexible small scale propellers

Pieter Maljaars[1], Nicola Grasso[2], Mirek Kaminski[3], Wim Lafeber[4]

[1,3] Ship Hydrodynamics and Structures Department, Delft University of Technology, Delft, The Netherlands
[2,4] MARIN, Wageningen, The Netherlands

ABSTRACT

This paper presents numerical and experimental results for the validation of a coupled Boundary Element Method (BEM)-Finite Element Method (FEM) simulation for uniform flows. In the first part of the paper the numerical models and the BEM-FEM coupling are presented. A large part of the paper is dedicated to the validation procedure which has been successfully applied to three small scale flexible propellers. Special attention has been paid to improve the accuracy of blade deformation measurements in a cavitation tunnel test setup. Results of tests on a flat plate show that accurate deformation measurements can be performed with a stereo camera system in combination with a Digital Image Correlation (DIC) technique. In the last part of the paper blade deformations calculated with the BEM-FEM coupling are compared to experimental results. Depending on the flow condition a good agreement between measured and calculated blade deformations was obtained.

Keywords

BEM-FEM coupling, Propeller deformation measurements, Digital Image Correlation, Hydro-elasticity, Composite propellers.

1 INTRODUCTION

The main purpose of this paper is to present a validation procedure which has been successfully applied to validate a BEM-FEM coupling for calculating the hydro-elastic response of flexible propellers in uniform flows. This paper is focused on the experiments and the obtained results, rather than the hydro-elastic analysis. The last decade many papers about flexible composite propellers have been published. The application of polymer composites as propeller material offers some intrinsic benefits like reduced corrosion, significant weight reduction, lower electric-magnetic signature, reduced vibration and improved damping properties. Due to the relatively low stiffness of polymer composites, composite propellers show a hydro-elastic response, meaning that the blade deformations influence the propeller loading and vice versa. Hence, the hydro-elastic response can be experimentally recorded by measuring a change in thrust and torque or by measuring the deformations. Usually, thrust, torque and blade deformations are measured and used for validation of the hydro-elastic calculations. There are several reasons why the blade displacement field is usually more suitable for validation purposes than thrust and torque values. Firstly, the displacement field is not an integrated value like thrust and torque. Secondly, blade displacements are unique for flexible propellers in a sense that they (almost) not exist in case of a traditional bronze propeller. Finally, changes in thrust and torque can be easily affected by unintended small deviations in propeller geometry introduced for instance by the manufacturing process. For this reason the present paper focuses, regarding the experiments, on the measurement of the blade displacements.

1.1 Literature

Several experimental studies with flexible propellers are presented in literature. The techniques applied in the measurement of the blade deformations of an operating propeller are laser tracking or optical techniques. Young (2008) measured the deformations of a propeller by a laser tracking technique and presented results for open water conditions. The accuracy of the measurements was too low to accurately predict the changes in pitch deformation of the stiffest propeller. Based on the presented results one can conclude that these pitch deformations should be in the order of one degree. More details about the propellers, testing and results used by Young (2008) can be found in Chen et al. (2006). This paper presents results of measurements and computations in a four-cycle wakefield. Compared to numerical results the magnitude of the measured pitch change was larger than predicted, however the trends were predicted well. Lee et al. (2014) used the experimental results presented by Chen et al. (2006) and Young (2008) for validation of their unsteady BEM-FEM coupling and found similar results.

Taketani et al. (2013) determined experimentally the propeller tip deformations in a uniform flow by manually measuring the displacements using image data. The full-field deformations of an operating propeller can be obtained with a stereo camera system in combination with DIC. This is a promising technique and has many advantages, including high resolution results, non-intrusive measurement, and good accuracy over a range of scales (Lv et al. 2013). A slightly different optical technique was successfully applied by Savio (2015) to measure propeller blade deformations with the blade surface covered with markers in place of the random

speckle pattern applied for DIC. According to Savio (2015) marker based techniques are more accurate than DIC, but this was not verified experimentally. Bunt and Lafeber (2011) describe the application of a DIC technique for measuring propeller blade deformations in a uniform flow. Maljaars and Dekker (2014) used the experimental data obtained by the experiment described in Bunt and Lafeber (2011) to validate a developed BEM-FEM coupling. It was concluded that the developed coupling can correctly predict the qualitative response of the flexible propeller. However, to quantify the accuracy of the coupling code, similar experiments had to be performed with an improved test setup. The experiments presented in this paper are performed with this improved setup.

1.2 Content

This paper is structured as follows: Section 2 presents the propellers, the FEM and BEM modelling and the steady BEM-FEM coupling. In Section 3 the validation procedure is described, with special attention to the cavitation tunnel test setup and the DIC measurements. In Section 4 numerical results obtained with the steady BEM-FEM coupling are compared to experimental results. Conclusions and recommendations are given in Section 5.

2 NUMERICAL MODELLING

2.1 The propellers

Four geometric identical propellers with a diameter 0.34m have been used for this work. The propellers differ with respect to material or laminate lay-up. The propellers and the blades have been numbered as follows for identification purposes:

- Bronze propeller: Isotropic NIAB material
- Epoxy propeller: Isotropic epoxy material.
- Propeller 45: [+45°/-45°] laminate lay-up.
- Propeller 90: [0°/90°] laminate lay-up.
- Blade number 1 and 2 are designated to the uppermost and bottommost blade respectively, see Figure 1.

The 0°direction of the laminae is parallel to the z-axis of the propeller blade coordinate system, as indicated in Figure 1. All the results presented in this paper are according to this reference system.

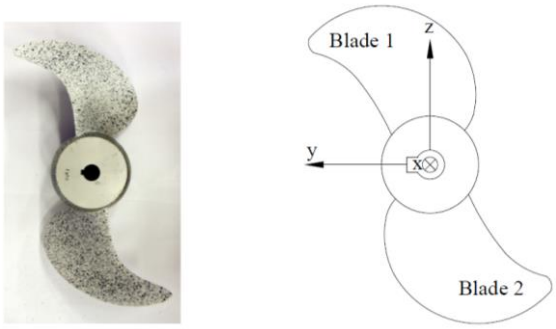

Figure 1: Picture of one of the small scale propellers and definition of the propeller coordinate system.

2.2 Finite element modelling of the propellers

This section briefly describes the FEM modelling of the small scale propellers. MSC Marc/Mentat has been used for FEM modelling and calculations. The FEM models consist of one propeller blade without the hub part. The stiffness contribution of the hub was modelled by a full clamping of the propeller blade at the blade-hub interface. The models have been discretised by quadratic solid elements. For the computations presented in this paper a 29×30×4 element distribution was used. This means that 29 elements are placed along the chord of the propeller (29 elements on both sides), 30 elements in radial direction and 4 elements in through-thickness direction, see Figure 2 for a picture of the FEM model.

Special attention has been given to the establishment of the material orientations in composite blades. In Chen et al. (2010) and Maljaars et al. (2017) the importance of a proper material orientation for doubly curved structures has been described. Standard commercial FEM software packages are usually not able to define unambiguously the material orientations in complex geometries (Chen et al. 2010).

Local element coordinate systems are usually available in FEM software packages. With this feature the through-thickness material orientation can be directed perpendicular to the outside surface of the elements. However, the alignment of the two other material axes will depend on the orientation of the element itself. This can result in an erroneous material orientation and a misprediction of the structural stiffness. To determine for each element the material orientation the approach presented in Maljaars et al. (2017) was applied. In this method the through thickness direction and the projection of the transverse laminate (90°) direction on the element surface was used to establish the material orientations per element. A more detailed description can be found in that paper.

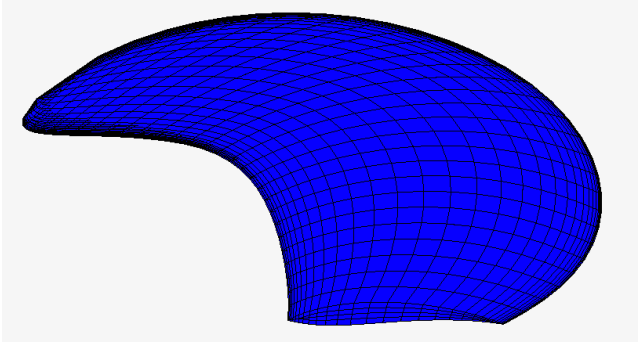

Figure 2: Picture of the FEM model.

2.3 Boundary element modelling of the propellers

For this work the BEM PROCAL, developed by the Maritime Research Institute Netherlands (MARIN), was used. PROCAL is based on potential flow theory. In PROCAL only the propeller surface has to be discretized. Results of panel sensitivity studies show that a 29×30 element distribution is sufficient to obtain an accurate solution. This means that the BEM and FEM solver

require a similar distribution of panels or elements on the propeller surface. This property has been used by applying identical mesh distributions in the FEM and the BEM model in order to avoid a transformation of pressures and structural response between the two grids.

2.4 Pressure correction at the tip

It can be assumed that the pressure difference between pressure and suction side at the propeller tip will be close to zero due the wing tip vortex. In general, with a potential flow solver a significant pressure difference at the tip will be computed. To correct for this the calculated pressures from a certain propeller radius are smoothed to a zero pressure coefficient at the tip. The default from where this tip pressure correction is applied, is 95% of the propeller radius. It will be shown in Section 4 that this radius has an important influence on the blade deformations.

2.5 BEM-FEM coupling for uniform flows

This subsection will explain how the BEM method PROCAL is coupled with the FEM software MSC Marc. The presented coupling is only applicable for steady problems, i.e. uniform flows. Figure 3 schematically depicts the coupling between the BEM solver PROCAL and the FEM software MSC Marc. In this coupling the following non-linear equation is solved:

$$F_{BEM}(u) + F_{Viscous}(u) + F_{Centrifugal} = Ku \quad (1)$$

where F_{BEM}, $F_{Viscous}$ and $F_{Centrifugal}$ denote nodal forces for hydrodynamic force, viscous forces and centrifugal forces respectively. K is the stiffness matrix. Essentially, all the parameters in Equation 1 are function of the displacements u. Since the blade deformations are relatively small, geometric linear elastic analyses are performed with the FEM solver.

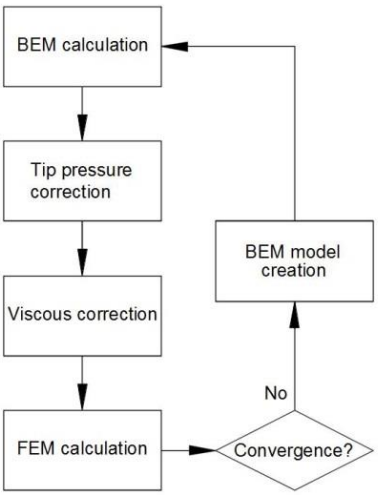

Figure 3: Flowchart of the coupling scheme.

The first step of the coupled BEM-FEM calculation is a PROCAL calculation on the undeformed geometry. The tip pressure correction are applied on the pressures obtained with PROCAL as explained in Section 2.4. Next, the viscous forces are calculated to account for frictional losses. Subsequently, the calculated pressures and viscous forces are used to calculate the structural response of the propeller blade. The structural displacements are used to construct a new propeller geometry. Then, the iteration loop starts again until a converged solution is obtained.

3 VALIDATION PROCEDURE

The goal of the presented work, is a validated BEM-FEM coupling which can be used to calculate the hydro-elastic response of flexible propellers in uniform flows. The hydro-elastic response is an interaction between the hydrodynamic loading and structural response. This means that the validation of the final numerical tool logically will start with a verification and validation of its main components, i.e. the hydrodynamic calculation and the structural response calculation. Therefore, the whole validation procedure was divided in the following parts:

- Checking of the propeller geometries.
- Validation of the FEM calculation and stiffness identification.
- Validation of the BEM calculation.
- Validation of the BEM-FEM coupling.

3.1 Checking of the propeller geometries

A verification of the actual geometry was conducted by comparing laser scanned images of the actual propellers to the design geometry. The result for one blade is depicted in Figure 4. A maximum distance between actual and design geometry of 1.340 mm at the tip was found. The color pattern on the blade indicates that the inaccuracy in the geometry is mainly due to rigid body offsets and rotation of the blade when glued into the hub, rather than the shape of blade itself. Similar results were obtained for the other blades.

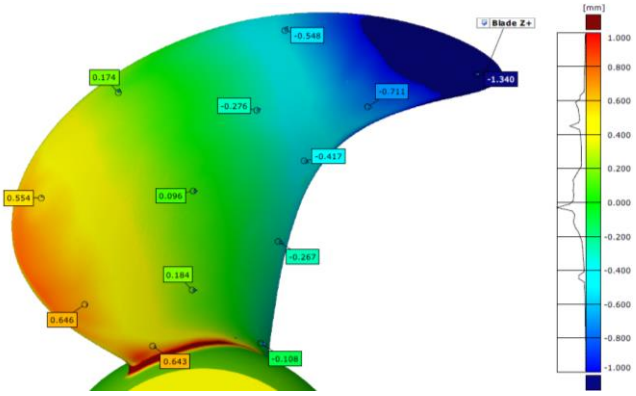

Figure 4: Difference in [mm] between design and as-build geometry for propeller 90, blade 1.

The influence of the difference between actual and design geometry on the blade forces was investigated by comparing results of BEM calculations obtained for the different geometries. Table 1 presents the thrust forces for design and as-build geometries for an advance coefficient of 0.375 and 0.85. The thrust is indicated between the brackets as percentage of the thrust obtained for the design geometry. Depending on the propeller blade and flow condition a significant difference in thrust force due to inaccuracies in the blade geometry can be observed.

Table 1: Thrust calculated for design and as-build geometries for two different flow conditions, left column J=0.375 and right column J=0.85.

	Va: 1.91 [m/s] N: 15 [Hz]	Va: 6.65 [m/s] N: 23 [Hz]
Design	758 N (100%)	815 N (100%)
Epoxy, blade 1	730 N (96.3%)	763 N (93.6%)
Epoxy, blade 2	727 N (95.9%)	780 N (95.7%)
Prop. 45, blade 1	793 N (105 %)	923 N (113 %)
Prop. 45, blade 2	747 N (98.5%)	802 N (98.4%)
Prop. 90, blade 1	755 N (99.6%)	826 N (101 %)
Prop. 90, blade 2	754 N (99.5%)	824 N (101 %)

3.2 Stiffness identification and validation of the FEM calculation

Between the design and the validation phase a complex blade manufacturing process took place. Therefore, it had be verified whether the propeller stiffness's are in accordance with the design values, and if not, what the actual values are. For that reason the propeller stiffness's were identified by means of a mixed numerical and experimental technique. In the applied approach results of static deformation tests were combined with results of FEM calculations.

An optimization algorithm was applied to minimize the difference between measured and calculated response by adapting the stiffness parameters in the FEM calculation. This approach was successfully applied on the blades of the composite propellers. For more details and the obtained results the reader is referred to Maljaars et al. (2017). The conclusion was that a relatively small improvement of the agreement between measured and calculated results can be obtained with the updated stiffness properties, since the actual material properties are already close to the design material properties. This is also confirmed by a verification study in which calculated and measured eigenfrequencies are compared. These results are presented in Table 2.

Table 2: Calculated and measured first and second blade eigenfrequencies in air [Hz].

	Measured	Design material properties	Calculated material properties
Epoxy, blade 1	310-454	318-460	n.a.
Epoxy, blade 2	310-454	318-460	n.a.
Prop. 45, blade 1	473-686	474-654	472-698
Prop. 45, blade 2	473-686	474-654	493-700
Prop. 90, blade 1	460-n.a.	498-763	514-758
Prop. 90, blade 2	487-n.a.	498-763	510-751

3.3 Validation of the BEM calculation

Besides the three flexible model scale propellers, the bronze equivalent was available as well. This propeller can be assumed as totally rigid. The open-water diagram of the bronze propeller has been experimentally determined and compared to the open water diagram calculated with the BEM PROCAL. These open water curves are depicted in Figure 5. This figure shows that especially for small advance coefficients the discrepancy between measured and calculated curves is relatively large, especially for the torque coefficient.

This discrepancy is caused by the relatively sharp leading edge that generates, especially for low advance coefficients, a strong leading edge vortex which is not included in the PROCAL calculation. For high advance coefficients the leading edge vortex disappears and a better agreement between the measured and the calculated open water diagram is obtained. Therefore, it was decided to carry out the validation experiments at high advance coefficients.

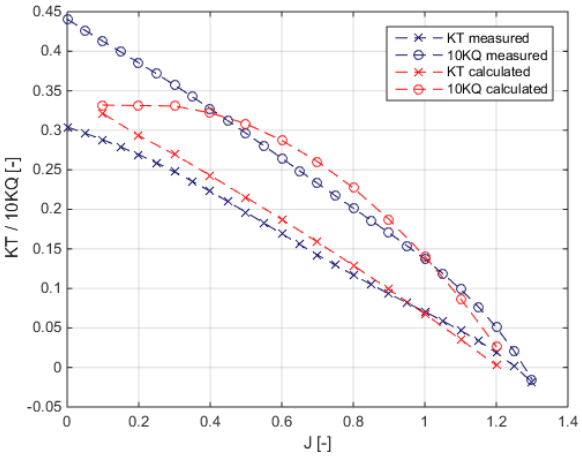

Figure 5: Calculated and measured open-water diagram.

3.4 Cavitation tunnel experiments

From the results obtained from the steps presented in the previous subsections the following conclusions can be drawn:

- The actual blade geometries differ from the design geometry. Therefore, for some propeller blades significant differences in blade loading between the actual and the design geometry has been found.
- Accurate structural responses have been obtained with the FE models.
- For this propeller geometry the best thrust and torque predictions are obtained for relatively high advance coefficients (between J 0.8 and 1.1).

Based on these conclusions and the fact that the blade deformations are relatively small, with a maximum of 5 mm at the tip for the epoxy propeller, it can be concluded that the thrust and torque values are not the most suitable quantities to assess the accuracy of the steady BEM-FEM coupling. The propeller blade deformations were used instead, meaning that an accurate recording of the

deformations of the operating propellers was required. Stereo-photography with a DIC technique was selected to measure the propeller blade deformations. With this system a very accurate recording of the complete 3D blade displacement field can be achieved.

3.4.1 Test setup

The cavitation tunnel of MARIN in Wageningen, The Netherlands, was selected as the testing facility. The propeller is mounted on the tunnel shaft, which is connected to an encoder. This encoder sends impulse signals used for the triggering of the strobe lights and the cameras. The test setup used in the cavitation tunnel can be summarized by Figure 6 and it consists of the following items:

- Two synchronized and calibrated cameras with FireWire interface; resolution: 1388 x 1038 pixels; maximum frame rate 16 fps at full resolution.
- Stroboscopic lights with flash duration in the micro second range. Flash duration is kept as short as possible to avoid motion blur at the blade tip.
- The shaft encoder mounted on the shaft, provides 360 pulses per revolution. A pulse selector is able to select one of these 360 pulses as a trigger, which is sent to the stroboscopes and the cameras. Therefore, a trigger can be supplied, with a resolution of one degree for every blade position. The cameras and the strobe are synchronized such that the strobe flash falls within the time frame the camera shutter is open.

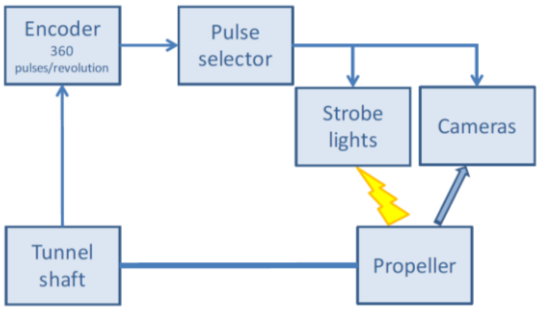

Figure 6: Cavitation tunnel setup diagram.

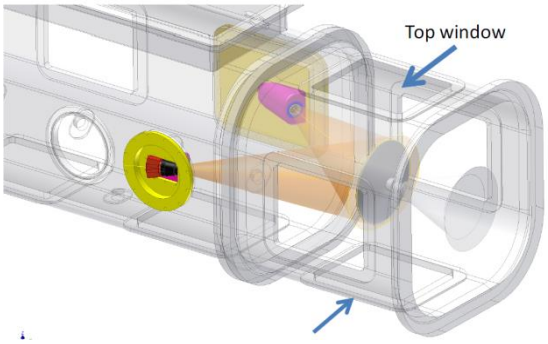

Figure 7: Proposed camera setup.

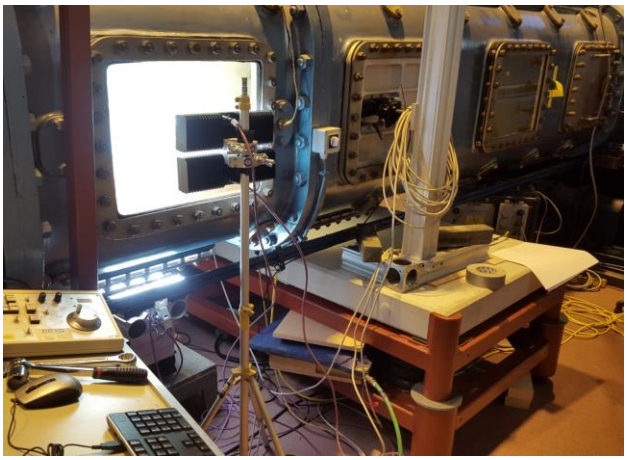

Figure 8: Picture of the cavitation tunnel test set-up.

Figure 7 shows the initially proposed camera setup. Two purposely built windows were mounted in place of the cavitation tunnel lateral windows to have an optimal camera view. Figure 8 shows a picture of the realized test setup. During the experiments one of the windows was moved to the bottom of the tunnel to further improve the view on the blade surfaces. In addition, the cameras were mounted on a vibration damping structure to ensure their absolute isolation from vibrations.

3.4.2 Measurement technique

The image data acquired with the calibrated stereo camera system are used to compute the blade deformations by means of DIC. DIC is a full-field image analysis method, based on grey value digital images that finds the displacements and deformations of an object in three dimensional space (Sutton et al. 2009). During the blade deformation the method tracks the grey value pattern from which the displacements of the object are calculated. This method can be used in several applications; in particular, it has been successfully applied for blade deflection measurements both in uniform flow in the cavitation tunnel and in behind ship model condition in the towing tank (Zondervan et al. 2017).

In order to use the DIC technique, the surface of the measured object must have a random speckle pattern with no preferred orientation and sufficiently high contrast. The size of the features in the pattern should be large enough to be distinguished as distinct features. If the material does not present naturally a usable speckle pattern, this must be applied through printing or painting.

With this technique very accurate measurements of the blade response were achieved. Several images for each blade position were acquired and image averaging was applied to filter out displacements resulting from high frequency vibrations of the propeller blade, and to remove eventual bubbles or particles in the water. The results were further post-processed and a procedure was applied to correct for rigid body motions induced by vibrations and deformations of the shaft.

3.4.3 DIC measurement accuracy

In order to estimate the obtained measurement accuracy a calibration test was performed. A rigid flat plate, with a speckle pattern, was mounted on the cavitation tunnel shaft. The displacements of the plate in axial direction due to different tunnel speeds (from 0 to 6 m/s) were measured. Given the stiffness of the plate, bending and shear deformations of the plate can be neglected. Therefore, the measured displacements are due to the compression of the tunnel shaft and are assumed constant over the plate area. The found distribution of the rigid displacement is an indicator of the measurement error. The distributions of the displacements over the plate area for two selected cases are shown in Figure 9.

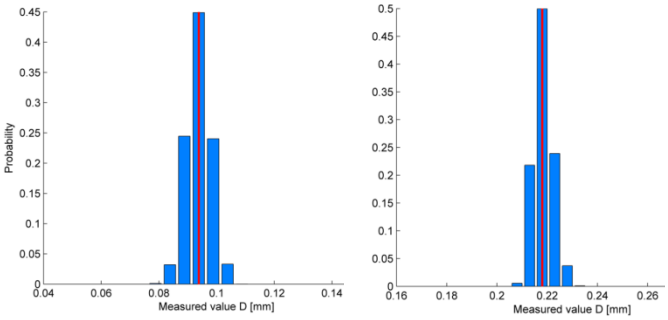

Figure 9: Distribution of measured displacements over the flat plate for tunnel speeds 4m/s (left) and 6m/s (right).

This figure shows that the 95% confidence interval is 0.02 mm. It is important to note that the measurement accuracy is a constant value: it does not vary with the magnitude of the displacement or the tunnel speed.

4 COMPARISON OF NUMERICAL AND EXPERIMENTAL RESULTS

Cavitation tunnel tests were performed with the three flexible propellers at different flow conditions. Deformation measurements were performed on both propeller blades. It is not practical to show all the results, therefore for each propeller only the results obtained for the highest and the lowest measured advance coefficient are presented. For the epoxy propeller the calculations were performed with the design material properties. For the composite propellers the material properties as obtained in Maljaars et al. (2017) were used. For each condition two calculations were performed with a different tip smoothing radius.

Table 3: Flow conditions and measured thrust values for measurement A to F.

Measurement	Va [m/s]	N [Hz]	J	Thrust [N]
A	1.88	15.0	0.37	680
B	6.73	23.3	0.85	727
C	1.92	15.0	0.38	680
D	6.75	23.3	0.85	705
E	1.98	15.0	0.39	670
F	6.74	23.3	0.85	691

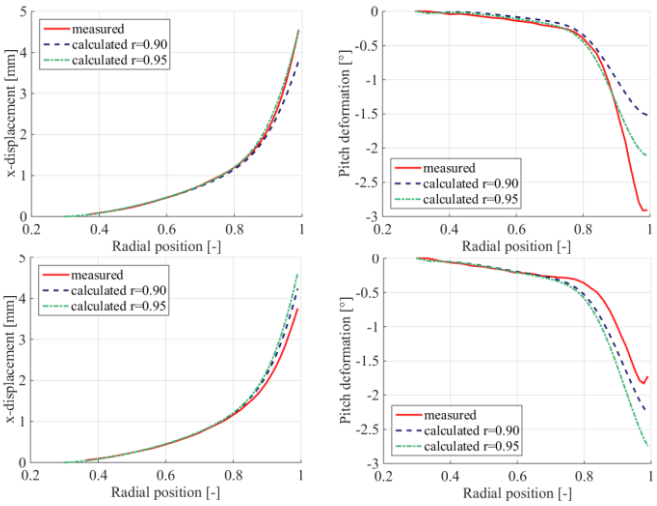

ure 10: Bending (left) and pitch (right) deformations of dchord points of the epoxy propeller, blade 1, obtained for urement A (top) and B (bottom).

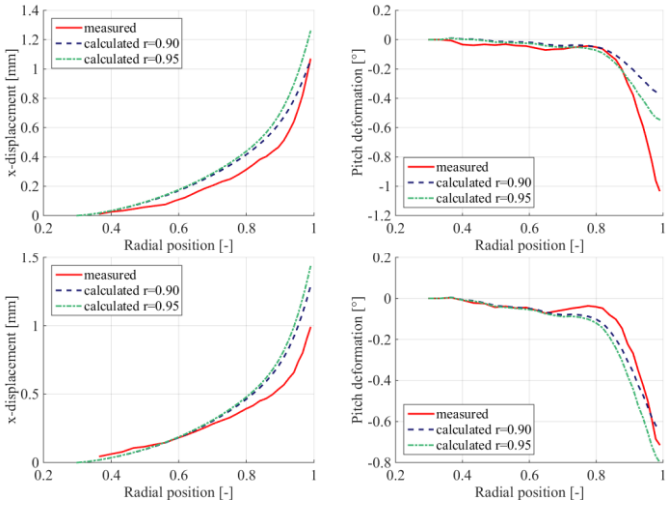

Figure 11: Bending (left) and pitch (right) deformations of midchord points of the propeller 45, blade 1, obtained for measurement C (top) and D (bottom).

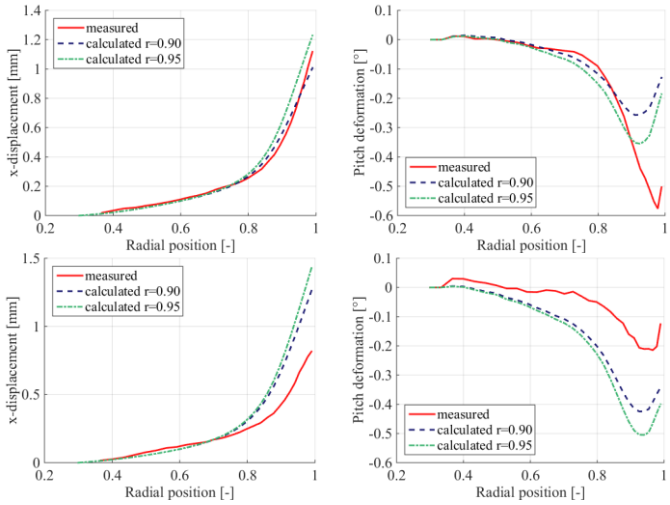

Figure 12: Bending (left) and pitch (right) deformations of midchord points of the propeller 90, blade 2, obtained for measurement E (top) and F (bottom).

Figure 11 to 13 show measured and calculated results for the flow conditions presented in Table 3. From all the figures it can be concluded that the radius used for the tip smoothing correction has a significant influence on the calculated blade deformations. That means that the deformations are very sensitive to small variations in propeller tip loading, while the difference in total blade thrust is only 2 to 3% when a tip smoothing radius of 0.90 or 0.95 has been used. The results show also that the best agreement between measured and calculated results is obtained for the high advance coefficient (bottom row of figures), which was expected as explained in Section 3.3. For these conditions (measurement B, D and F) the BEM-FEM calculation slightly over predicts the response. For the low advance coefficient a good agreement between measured and calculated bending response is obtained, but for these conditions the measured pitch deformations are much larger than calculated. This indicates a significant difference between calculated and actual pressure distribution. The most likely cause is the leading edge vortex as explained in Section 3.3. It can be concluded that the best agreement between measurements and calculations is obtained for the epoxy propeller and propeller 45.

5 CONCLUSIONS AND RECOMMENDATIONS

This paper presents a multi-stage validation procedure with four small scale propellers of same size and geometry which was successfully applied for the validation of a coupled BEM-FEM calculation for steady flows. First, the accuracy of the as-build propeller geometries was checked. Results of calculations show, depending on propeller and flow condition, that the inaccuracies in propeller geometry have a significant influence on the blade loading. Secondly, static and dynamic experiments were conducted to validate the FEM modelling and to adjust the material properties such that the agreement between results of FEM calculations and measurements is improved. The BEM modelling was validated by performing open-water measurements with a bronze propeller. It can be concluded that especially for low advance coefficients large differences between measured and calculated thrust and torque were obtained, likely caused by a strong leading edge vortex. Therefore, it is recommended to re-execute the validation procedure with another propeller which is more appropriate for a potential flow solver. Finally, blade deformation measurements were performed in the cavitation tunnel of MARIN by using a calibrated stereo camera system in combination with DIC. Tests on a flat plate show that with this measurement technique an accuracy of 0.02 mm can be achieved. The obtained accuracy is independent of the flow speed or the magnitude of the displacements.

In Section 4, numerical and experimental results are compared. It can be concluded that for the high advance coefficient the trends in bending and pitch deformations are very well predicted by the BEM-FEM coupling. The largest differences between calculations and measurements are observed for the lowest advance coefficient, most likely due to the leading edge vortex. It is recommended to investigate this by performing RANS computations. Overall, it can be concluded that the presented approach results in accurate blade deformation measurements and a successful validation of the steady BEM-FEM coupling. The next step is to develop an unsteady BEM-FEM coupling for non-uniform flows and to validate this simulation with blade deformation measurements of a propeller behind a wakefield.

ACKNOWLEDGEMENTS

The authors gratefully acknowledge the Defence Materiel Organisation, Maritime Research Institute Netherlands, Wärtsilä Netherlands B.V. and Stichting voor de Technische Wetenschappen (project number 13278) for their financial support. The authors gratefully thank the Cooperative Research Ships for their cooperation in this work and for using the BEM software PROCAL.

REFERENCES

Bunt van den, E. and Lafeber, W. (2011). "Optical Measurement Techniques in Model Testing," Advanced Model Measurement Technology, Newcastle.

Chen, J., Hallet, S. and Wisnom, M. (2010). "Modelling complex geometry using solid finite element meshes with correct composite material orientations," Computers and Structures, 88, 602-609.

Chen, B., Neely, S., Michael, T., Gowing, S., Szwerc, R., Buchler, D. and Schult, R. (2006). "Design, Fabrication and Testing of Pitch-Adapting (Flexible) Composite Propellers," The SNAME propeller/shafting symposium, Williamsburg VA.

Lee, H., Song, M.C., Suh, J.C. and Chang, B.J. (2014). "Hydro-elastic Analysis of Marine Propellers based on a BEM-FEM Coupled FSI Algorithm," International Journal of Naval Architecture and Ocean Engineering, 6, 562-577.

Lv, P., Prothi, S., Mohd-Zawawi, F., Benard, E. and Morlier, J. (2013). "Study of A Flexible Blade for Optimized Proprotor," ERCOFTAC International Symposium, Mykonos, Greece.

Maljaars, P.J. and Dekker, J.A. (2014). "Hydro-elastic Analysis of Flexible Marine Propellers," Maritime Technology and Engineering – Edited by Guedes Soares and Santos, 705-715.

Maljaars, P.J., Kaminski, M.L. and Besten den, J.H. (2017). "Finite Element Modelling and Model Updating of Small Scale Composite Propellers," submitted to Journal of Composite Structures.

Sutton, J., Ortue, J. and Schreier, H. (2009). "Image Correlation for Shape, Motion and Deformation Measurements: Basic Concepts, Theory and Applications," Boston 1st Edition.

Savio, L. (2015). "Measurements of the Deflection of a Fflexible Propeller Blade by means of Stereo

Imaging," Fourth International Symposium on Marine Propulsors, Austin, Texas, USA.

Taketani, T., Kimura, K., Ando. S. and Yamamoto, K. (2013). "Study on Performance of a Ship Propeller Using a Composite Material," Third International Symposium on Marine Propulsors, Launceston, Tasmania, Australia.

Young, Y.L. (2008). "Fluid-Structure Interaction Analysis of Flexible Composite Marine Propellers," Journal of Fluids and Structures, 24, 799-818.

Zondervan, G. J., Grasso, N., and Lafeber, W. (2017). "Hydrodynamic design and model testing techniques for composite ship propellers" Proceedings of the Fifth International Symposium on Marine Propulsion (SMP'17), Espoo, Finland.

DISCUSSION

Question from Luca Savio

The experimental results show different levels of smoothness of the curves. Have the authors investigated why?

Author's closure

It is true that the experimental results presented for the epoxy propeller in Figure 10 are smoother than the measured curves as presented in Figure 11 and 12 for the composite blades. The explanation is the difference in magnitude of the deformations. Due to the lower blade stiffness, the deformations of the epoxy propeller is more or less three times larger than the deformations of the composite propellers and therefore the measurement inaccuracies are relatively smaller for the epoxy blade than for the composite blades.